

Magnet settings for E93-038

Simon Taylor

July 10, 2000

This note accumulates various information about the Charybdis dipole magnet.

1 Magnet settings for 8.25in and 10in gaps

The current settings are determined by the integrated Bdl needed to precess the neutron's spin by 90° . The precession angle χ is related to the field integral according to

$$\chi = \frac{-1.913e \int Bdl}{M_p \beta_n c}, \quad (1)$$

where β_n is the speed of the neutron in units of c , M_p is the mass of the proton, $e = 1.6 \times 10^{-19}$ C. Computing β_n in terms of Q^2 , the magnitude of the field integral needed for a precession angle $\chi = \pi/2$ is given by

$$\left| \int Bdl \right| = \frac{\pi}{2} \left(\frac{M_p c}{1.913e} \right) \frac{\sqrt{Q^4 + 4M_n^2 Q^2}}{Q^2 + 2M_n^2}. \quad (2)$$

Q^2 (GeV/c^2)	$ \int Bdl $ (Tm)	I(A)
0.415	1.5084	417.5
0.451	1.5537	427.3
1.146	2.0442	586.2
1.484	2.1580	636.8

Table 1: 10" gap, no field clamps

Q^2 (GeV/c^2)	$ \int B dl $ (Tm)	I(A)
0.415	1.5084	373.9
0.451	1.5537	385.6
1.146	2.0442	542.1
1.484	2.1580	593.3

Table 2: 8.25" gap, 2" field clamps

Q^2 (GeV/c^2)	$ \int B dl $ (Tm)	I(A)
0.415	1.5084	349.4
0.451	1.5537	360.5
1.146	2.0442	489.5
1.484	2.1580	526.2

Table 3: 8.25" gap, no field clamps

2 TOSCA calculations

The plan is to wire the coils in parallel. Although the power supply current can be regulated very well, small changes in the resistance in one or other of the coils can change the relative current densities in the coils. This will affect the magnetic field at some level and so change the $\int B dl$ the neutrons see as they pass through the magnet gap. In order to assess the magnitude of this potential problem, TOSCA calculations were performed for the 8" gap, no field clamp configuration in which the difference in current density between the upper and lower coils was 5% of the power supply current, which was kept fixed. The lower coil (-y direction) had the higher current. Figures 1 and 2 show the difference between the magnitude of the field for the symmetric case and the asymmetric case relative to the midplane field for the symmetric case for the three magnet excitations for transverse profiles at the magnet center and near the pole edge ($z=61.2$ cm), respectively. The magnitude of the relative difference rises as the x and z position moves away from the center of the magnet. Figures 3 and 4 show the relative difference for longitudinal profiles at the center ($x=0$ cm) and the edge ($x=25.7$ cm), respectively. For the magnet center, the difference is small within the magnet (up to about 50 cm in z) but becomes appreciable for the fringe field. The maximum relative difference is about 2.3% for $y=+10$ cm and -3.4% for $y=-10$ cm. For

the $x=25.7$ cm case, the relative difference is relatively flat ($\sim 0.5\text{--}0.75\%$ for $y=+10$ cm and $\sim -0.7\text{--}-0.8\%$ for $y=-10$ cm) inside the magnet but increases in magnitude outside the pole tips. For this case the maximum relative difference is about -3.8% for $y=-10$ cm and $+2.5\%$ for $y=+10$ cm near the end of the calculation range. Figures 5 and 6 plot the difference between the magnitude of the field for $y=+10$ cm and $y=-10$ cm for the asymmetric current densities normalized to the field in the midplane of the magnet for the symmetric current density case as a function of position in x and z . The first column in each figure shows the longitudinal profiles as a function of magnet excitation. Again, the relative differences are largest in the fringe field (toward large z). The second column in each figure shows the transverse profile as a function of magnet excitation. The difference becomes appreciable as x moves away from the center of the magnet.

The difference in the field integral is most relevant for the experimental program.

The TOSCA calculations for the highest magnet excitation suggest that the magnitude of the fringe field in the region of the photo-multiplier tubes would be less than 2 gauss in the absence of the steel collimator, as shown in figure 7.

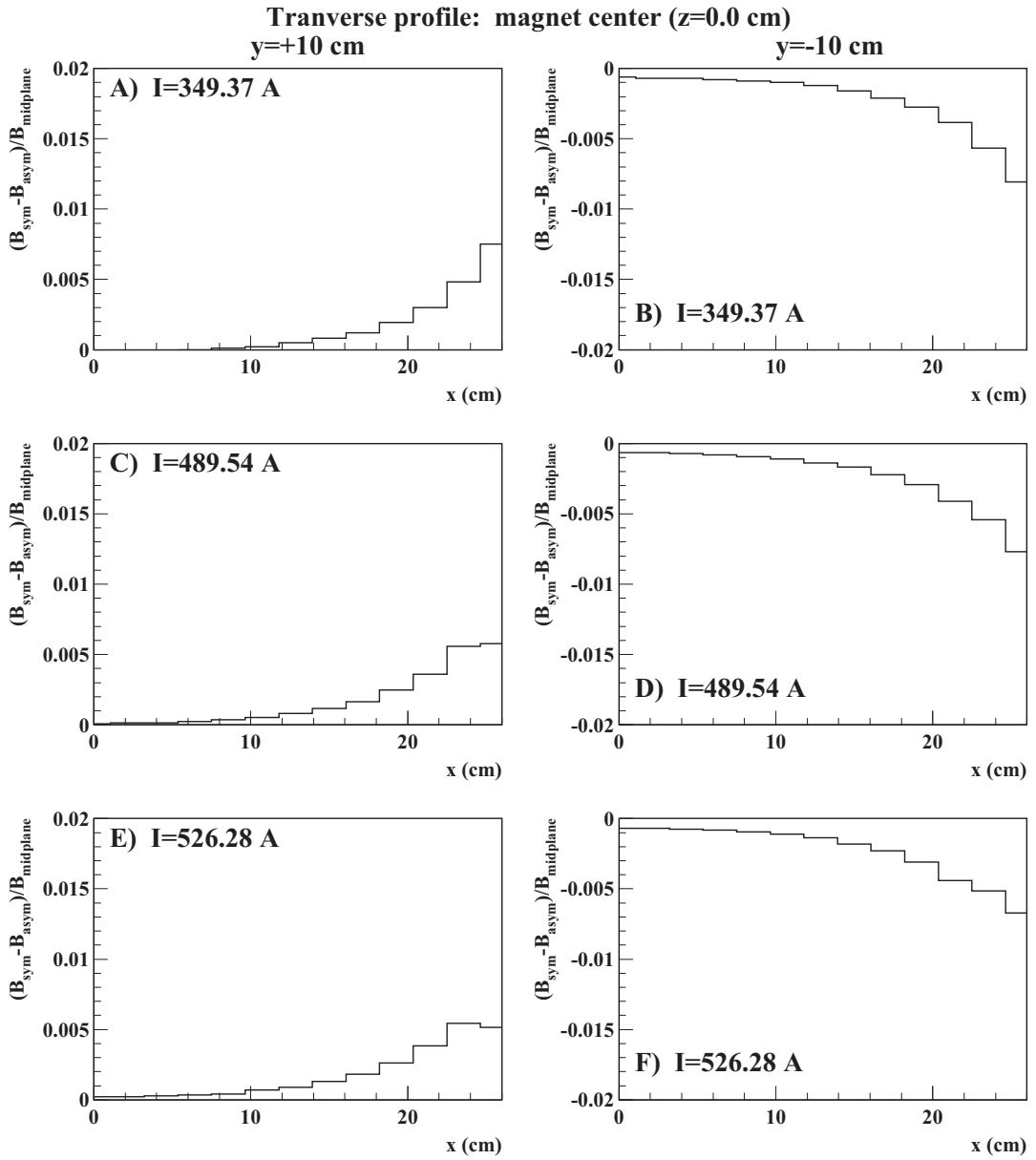


Figure 1: Transverse profiles for $z=0$ cm as a function of PSU current I and y -position. A) $I=349.37$ A, $y=+10$ cm; B) $I=349.37$ A, $y=-10$ cm; C) $I=489.54$ A, $y=+10$ cm; D) $I=489.54$ A, $y=-10$ cm; E) $I=526.28$ A, $y=+10$ cm; F) $I=526.28$ A, $y=-10$ cm.

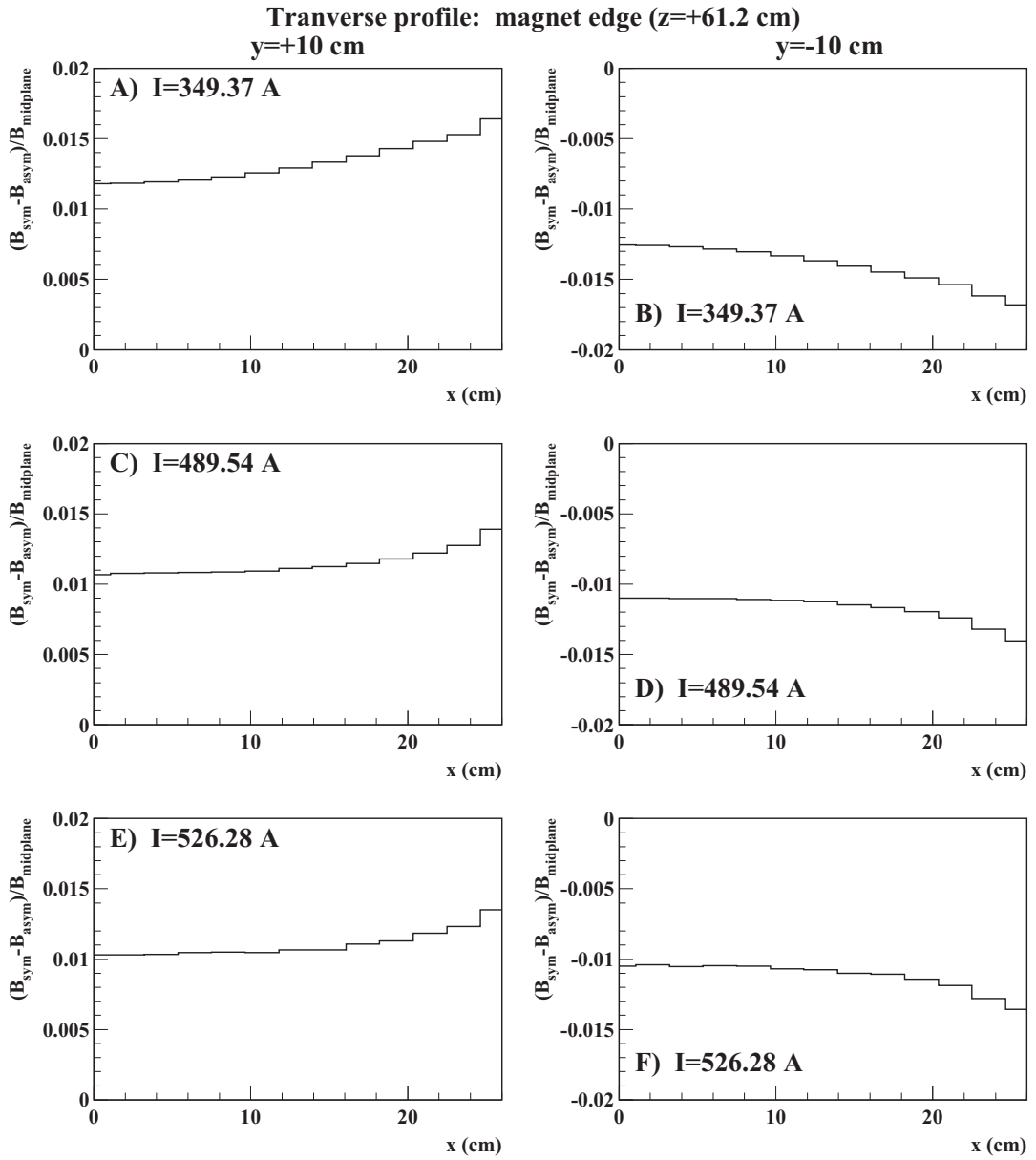


Figure 2: Transverse profiles for $z=61.2$ cm as a function of PSU current I and y -position. A) $I=349.37$ A, $y=+10$ cm; B) $I=349.37$ A, $y=-10$ cm; C) $I=489.54$ A, $y=+10$ cm; D) $I=489.54$ A, $y=-10$ cm; E) $I=526.28$ A, $y=+10$ cm; F) $I=526.28$ A, $y=-10$ cm.

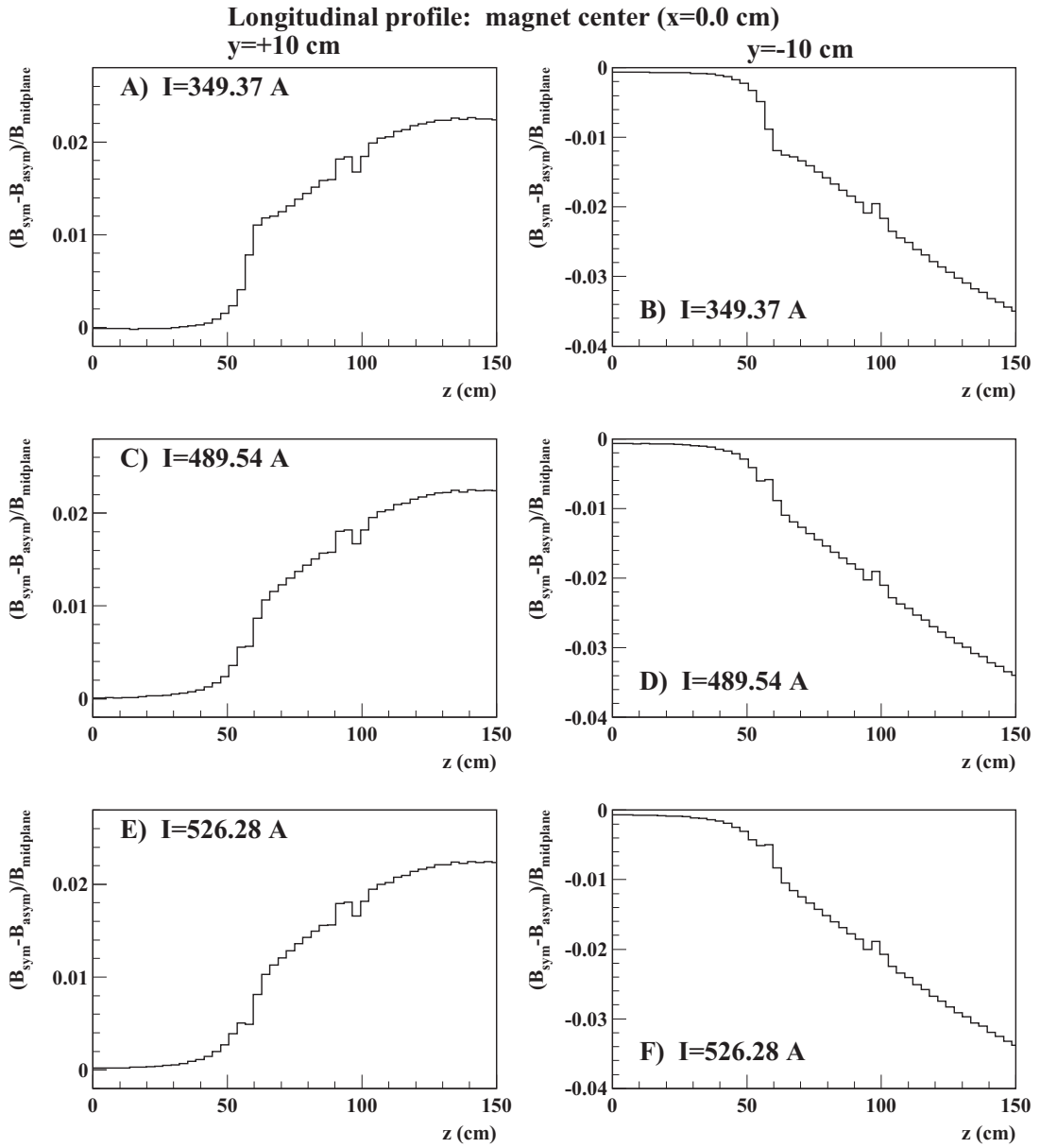


Figure 3: Longitudinal profiles for $x=0$ cm as a function of PSU current I and y -position. A) $I=349.37$ A, $y=+10$ cm; B) $I=349.37$ A, $y=-10$ cm; C) $I=489.54$ A, $y=+10$ cm; D) $I=489.54$ A, $y=-10$ cm; E) $I=526.28$ A, $y=+10$ cm; F) $I=526.28$ A, $y=-10$ cm.

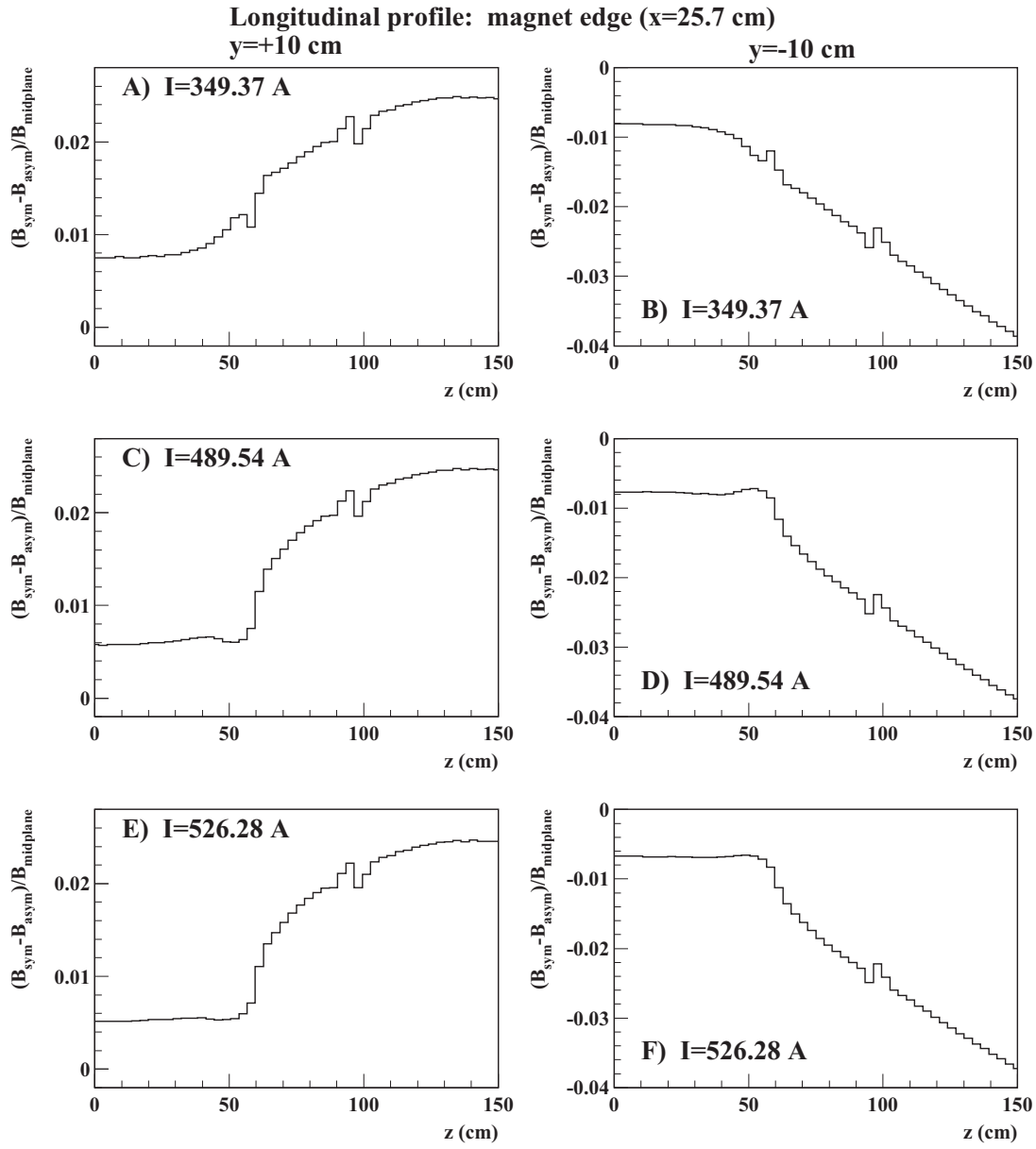


Figure 4: Longitudinal profiles for $x=25.7$ cm as a function of PSU current I and y -position. A) $I=349.37$ A, $y=+10$ cm; B) $I=349.37$ A, $y=-10$ cm; C) $I=489.54$ A, $y=+10$ cm; D) $I=489.54$ A, $y=-10$ cm; E) $I=526.28$ A, $y=+10$ cm; F) $I=526.28$ A, $y=-10$ cm.

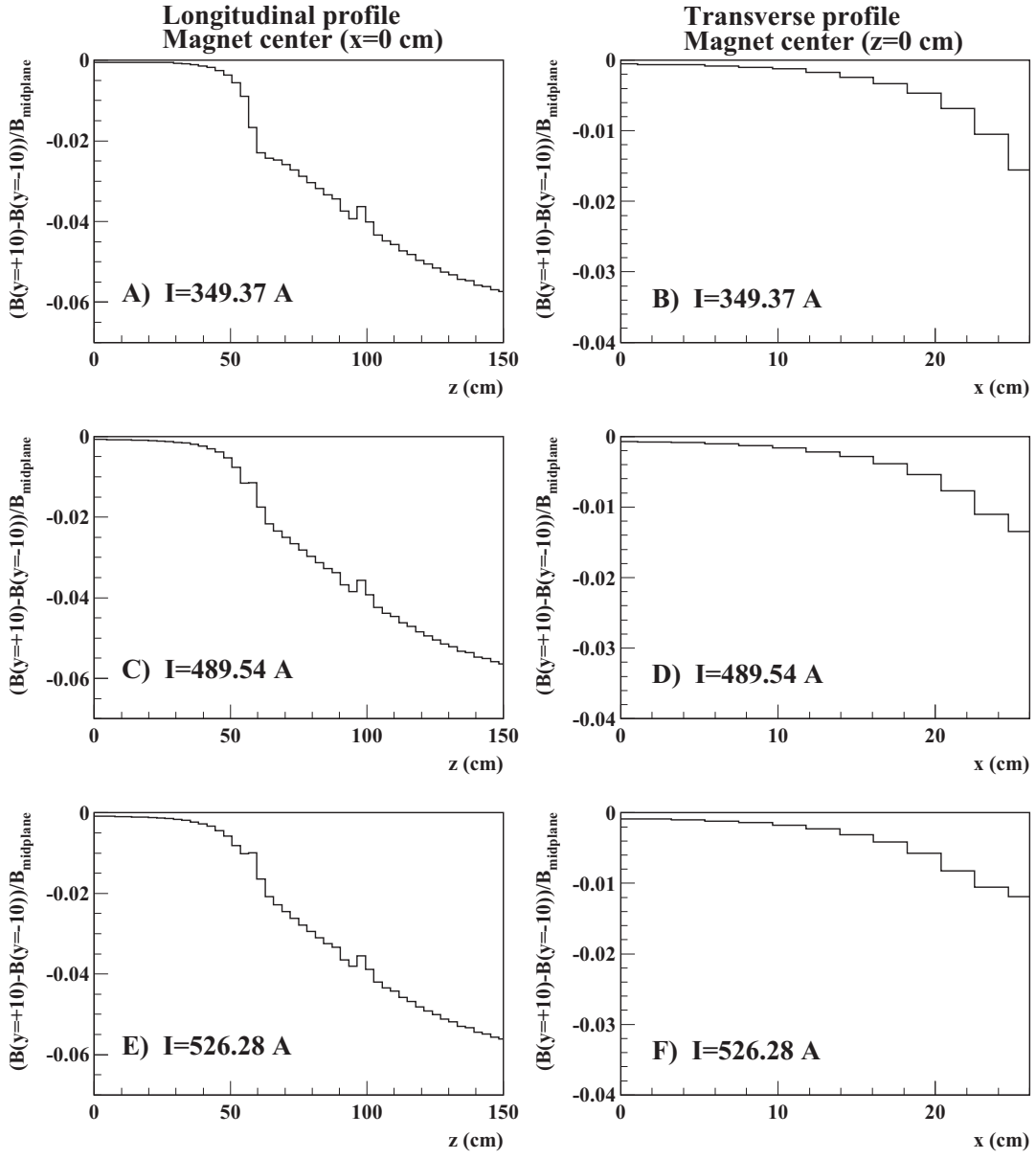


Figure 5: A) Longitudinal profile for $I=349.37$ A; B) Transverse profile for $I=349.37$ A; C) Longitudinal profile for $I=489.54$ A; D) Transverse profile for $I=489.54$ A; E) Longitudinal profile for $I=526.28$ A; F) Transverse profile for $I=526.28$ A.

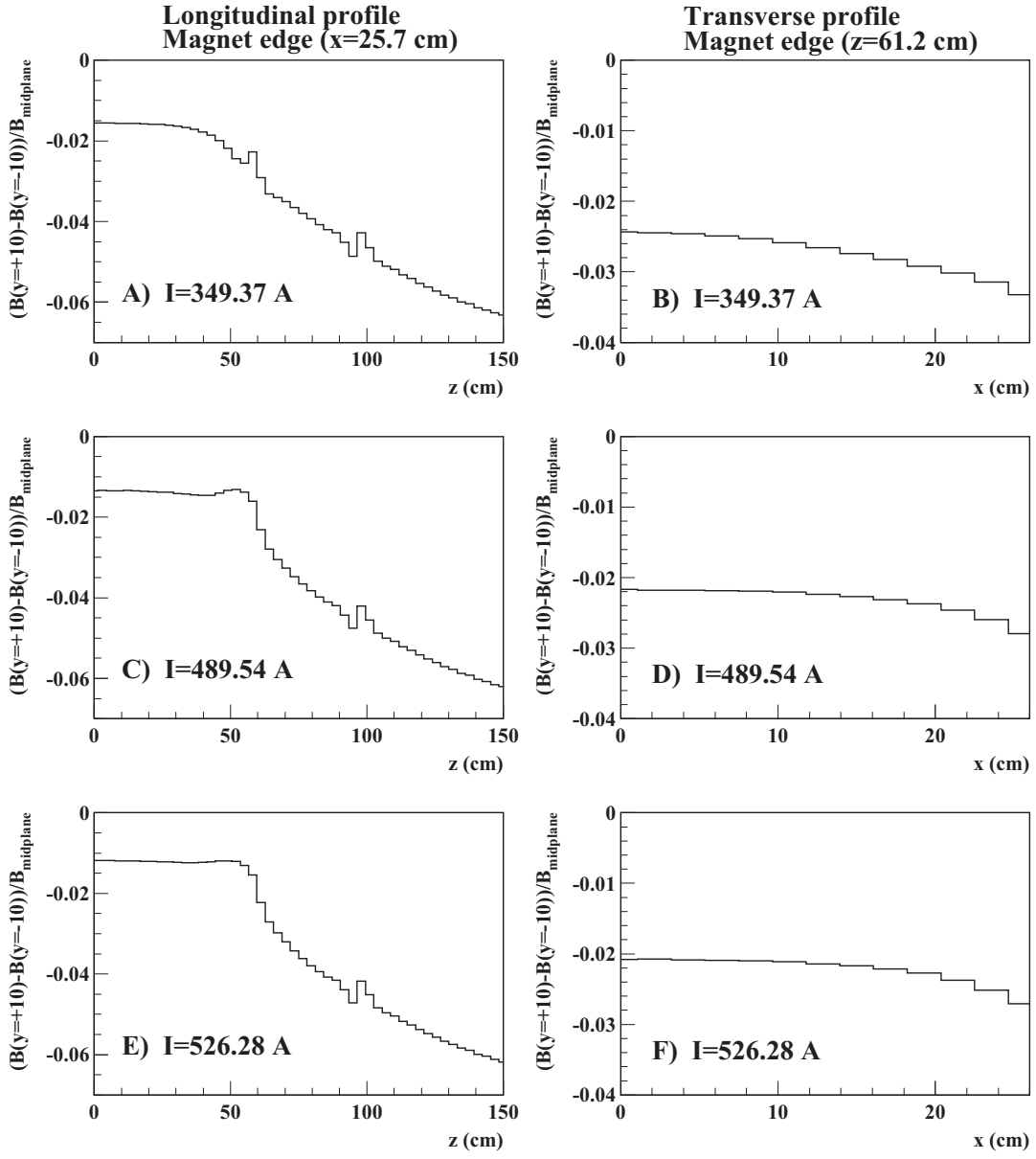


Figure 6: A) Longitudinal profile for $I=349.37$ A; B) Transverse profile for $I=349.37$ A; C) Longitudinal profile for $I=489.54$ A; D) Transverse profile for $I=489.54$ A; E) Longitudinal profile for $I=526.28$ A; F) Transverse profile for $I=526.28$ A.

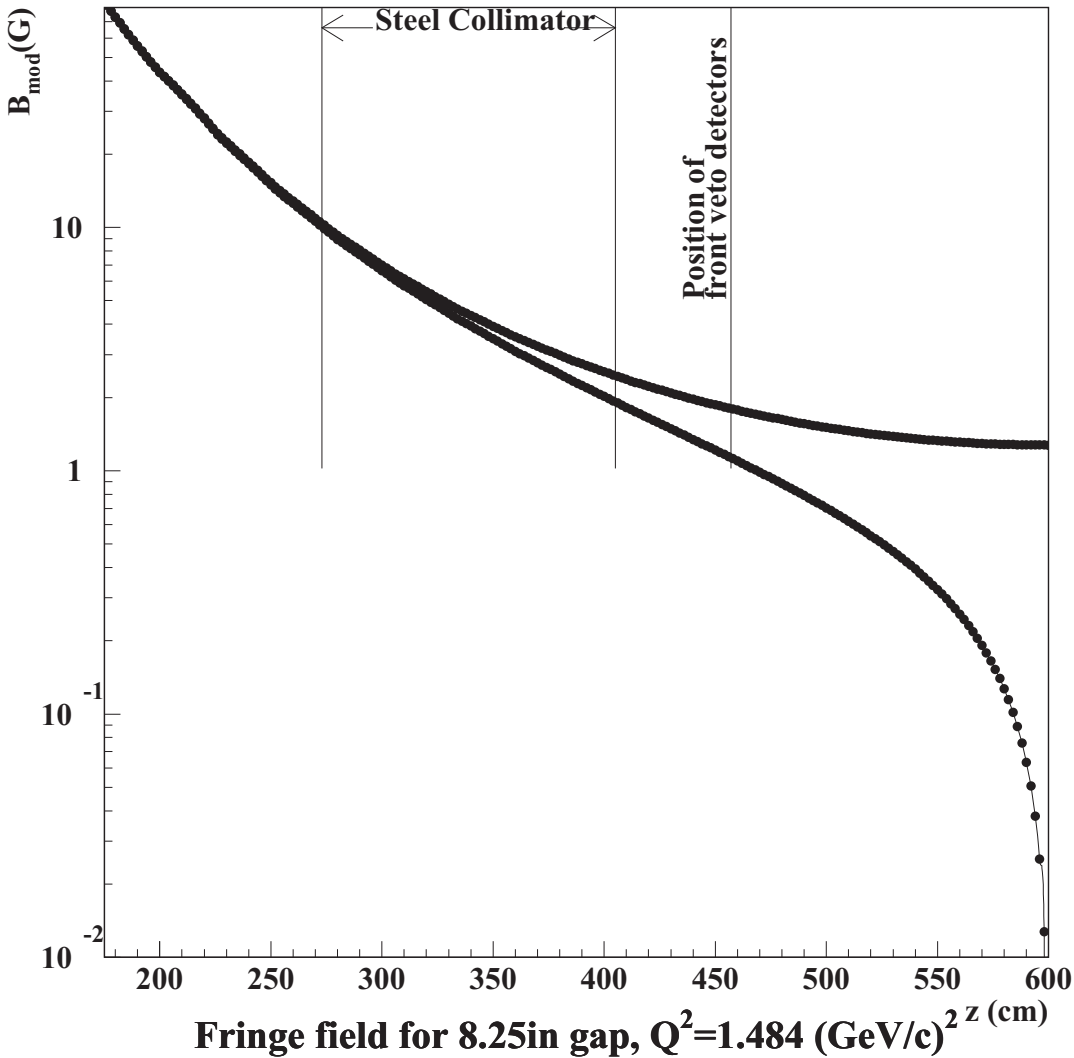


Figure 7: Fringe field for $Q^2 = 1.484 (\text{GeV}/c)^2$.